

Proceeding Paper

Three-dimensional singularity analysis for a magneto-electro-elastic wedge

* C. S. Huang¹⁾ and C. N. Hu²⁾

^{1), 2)} *National Chiao Tung University, Hsinchu, Taiwan*

¹⁾ cshuang@mail.nctu.edu.tw

ABSTRACT

Three-dimensional asymptotic solutions are established for magneto-electro-elastic (MEE) singularities in MEE wedges. The solutions are obtained by combining an eigenfunction expansion approach with the power series solution method to solve three-dimensional equilibrium equations and Maxwell's equations in terms of mechanical displacement components and electric and magnetic potentials. The MEE material is assumed to be transversely isotropic and its polarization direction is not necessarily parallel to the thickness direction of wedge. The correctness of the proposed solutions is confirmed by comparing with the published result for a special case. The developed solutions are further employed to examine the effects of the direction of polarization, the configuration of wedge and the material components on the orders of the singularities in wedges.

1. INTRODUCTION

Magneto-electro-elastic (MEE) materials can exchange mechanical, electric and magnetic forms of energy among each other and have been widely used in electronic devices, including acoustic actuators, magneto-electro-mechanical transducers, electric field tunable microwave resonators, highly sensitive magnetic or electric current sensors and other smart structures. It is interesting and important to investigate geometrically-induced magneto-electro-elastic singularities in wedges because such singularities normally initiate cracking and worsen the functioning of structures.

Lots of studies on geometrically-induced stress singularities in elastic wedges have been carried out, and most of them were collected in the excellent review paper by Sinclair (2004). Williams (1952a, b) was at the forefront of investigating stress singularities at the vertex of an elastic wedge under extension or bending. Following his work, numerous studies have been performed on elastic wedges, which are based on

¹⁾ Professor

²⁾ Graduate Student

plane elasticity theory (Bogy and Wang 1971, Dempsey and Sinclair 1979, Ting and Chou 1981, Lin and Sung 1998), classical plate theory (Rao 1971, Ojikutu *et al.* 1984, Huang and Chang 2007), first-order shear deformation plate theory (Burton and Sinclair 1986, Huang 2003, McGee and Kim 2005), third-order plate theory (Huang 2002), and higher-order plate theory (Huang 2004), and three-dimensional elasticity theory (Hartranft and Sih 1969, Xie and Chaudhuri 1997).

In the last two decades, the geometrically-induced singularities in piezoelectric wedges have caught the attention of researchers. Most of investigations make the plane strain assumption or the generalized plane deformation assumption. Using the plane strain assumption, Xu and Rajapakse (2000) extended Lekhnitskii's complex potential functions for in-plane stresses and electric displacement components to examine the singularities at the vertex of a piezoelectric wedge, while Shang and Kitamura (2005) utilized a modified version of the general solution of Wang and Zheng (1995). Hwu and Ikeda (2008) made the generalized plane strain assumption and proposed an extended Stroh formulation to investigate the in-plane and out-of-plane electroelastic singularities in wedges. Chue and his co-workers (2002, 2003 and 2004) adopted the generalized plane deformation assumption and conducted a series of analytical studies of geometrically-induced electroelastic singularities by using the extended Lekhnitskii formulation or the Mellin transform. By using various finite element approaches, Scherzer and Kuna (2004), Chen *et al.* (2006) and Chen and Ping (2007) examined in-plane singular electroelastic states at the vertex of a wedge. Based on three-dimensional piezoelectricity theory, Huang and Hu (2013) developed asymptotic solutions to comprehensively investigate the geometrically-induced electroelastic singularities at the vertex of a wedge whose direction of polarization is arbitrary.

There are only few studies conducted for geometrically-induced singularities in MEE wedges. These published works considered wedges subjected to anti-plane deformation and in-plane electric and magnetic fields with assuming that all of the physical quantities were independent of the coordinates along the thickness. To determine the singularities at the vertex of a bi-material MEE wedge, Liu and Chue (2006) employed the Mellin transform, and Sue *et al.* (2007) used the complex potential function with eigenfunction expansion method. Liu (2009) further extended the solution of Liu and Chue (2006) to examine the singularities at the apex of an MEE wedge-junction structure, with considering the air effect.

The main purpose of the work is based on three-dimensional magneto-electro-elasticity theory to develop an asymptotic solution to investigate geometrically-induced singularities in MEE wedges. Since the direction of polarization of an MEE wedge can be arbitrary in space, the in-plane components of displacement, electric and magnetic fields are generally coupled with the out-of-plane components, which much complicates the solution. An eigenfunction expansion approach with the power series solution technique and domain decomposition is adopted to establish the asymptotic solutions by directly solving the three-dimensional equations of motion and Maxwell's equations in terms of mechanical displacement components and electric and magnetic potentials. The correctness of the proposed solutions is confirmed by comparing the order of MEE singularities with the published result for a wedge under anti-plane deformation and in-plane electric and magnetic fields. The proposed solutions

are further applied to study the effects of the direction of polarization, vertex angle, and boundary conditions on the singularities in MEE wedges.

2. CONSTRUCTION OF ASYMPTOTIC SOLUTION

Consider a rectilinearly anisotropic MEE wedge with vertex angle β , shown in Fig. 1, where the $\bar{x}\text{-}\bar{y}\text{-}\bar{z}$ coordinate system is used to describe the material anisotropy, and the $x\text{-}y\text{-}z$ coordinate system is used to describe the geometry of the wedge. It is easy to solve for the MEE singularities at the vertex of the wedge in the cylindrical coordinate system (r, θ, z) given in Fig. 1. The material properties defined in the $\bar{x}\text{-}\bar{y}\text{-}\bar{z}$ coordinate system have to transform to the cylindrical coordinate system, and linear constitutive equations in the cylindrical coordinate system can be expressed as

$$\{\sigma\} = [c]\{\varepsilon\} - [e]^T \{E\} - [d]^T \{H\} \quad (1a)$$

$$\{D\} = [e]\{\varepsilon\} + [\eta]\{E\} + [g]\{H\} \quad (1b)$$

$$\{B\} = [d]\{\varepsilon\} + [g]\{E\} + [\mu]\{H\} \quad (1c)$$

where $\{\sigma\}$, $\{\varepsilon\}$, $\{D\}$, $\{B\}$, $\{E\}$ and $\{H\}$ are the stress, strain, electric displacement, magnetic flux, electric field and magnetic field vectors, respectively; $[c]$, $[e]$, $[d]$, $[\eta]$, $[\mu]$ and $[g]$ are the elastic stiffness constant, piezoelectric coefficient, piezomagnetic coefficient, dielectric constant, magnetic permeability and magnetoelectric coefficient matrices, respectively.

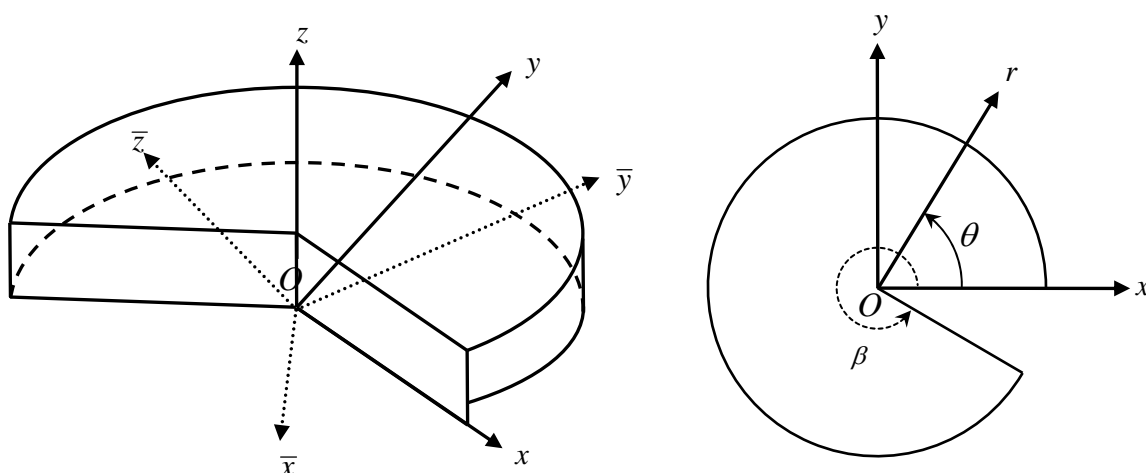


Fig. 1 Coordinate systems for a wedge

Following the eigenfunction expansion approach, which Hartranft and Sih(1969) used for 3D elastic wedges, the mechanical displacements, electric potential and magnetic potential are expressed as

$$\begin{aligned}
 u_r(r, \theta, z, t) &= \left[\sum_{m=1}^{\infty} \sum_{n=0}^{\infty} r^{\lambda_m+n} \hat{U}_n^{(m)}(\theta, z) \right] e^{i\omega t}, \quad u_\theta(r, \theta, z, t) = \left[\sum_{m=1}^{\infty} \sum_{n=0}^{\infty} r^{\lambda_m+n} \hat{V}_n^{(m)}(\theta, z) \right] e^{i\omega t}, \\
 u_z(r, \theta, z, t) &= \left[\sum_{m=1}^{\infty} \sum_{n=0}^{\infty} r^{\lambda_m+n} \hat{W}_n^{(m)}(\theta, z) \right] e^{i\omega t}, \quad \phi(r, \theta, z, t) = \left[\sum_{m=1}^{\infty} \sum_{n=0}^{\infty} r^{\lambda_m+n} \hat{\Phi}_n^{(m)}(\theta, z) \right] e^{i\omega t}, \\
 \psi(r, \theta, z, t) &= \left[\sum_{m=1}^{\infty} \sum_{n=0}^{\infty} r^{\lambda_m+n} \hat{\Psi}_n^{(m)}(\theta, z) \right] e^{i\omega t}, \quad (2)
 \end{aligned}$$

where u_i ($i=r, \theta, z$) is the displacement component in the i direction, and electric potential and magnetic potential are related to electric and magnetic fields, respectively, by

$$E_r = -\frac{\partial \phi}{\partial r}, \quad E_\theta = -\frac{1}{r} \frac{\partial \phi}{\partial \theta}, \quad E_z = -\frac{\partial \phi}{\partial z}, \quad H_r = -\frac{\partial \psi}{\partial r}, \quad H_\theta = -\frac{1}{r} \frac{\partial \psi}{\partial \theta}, \quad \text{and } H_z = -\frac{\partial \psi}{\partial z}. \quad (3)$$

The characteristic values λ_m may be real or complex for MEE wedges. To ensure the finite displacements, electric field and magnetic field at $r = 0$, the real part of λ_m is required to be positive. Notably, when the real part of λ_m ($\text{Re}[\lambda_m]$) is less than unity, the order of the singularities of stress, electric displacement and magnetic flux is $\text{Re}[\lambda_m]-1$.

Substituting Eqs. (2) into the equations of motion and Maxwell's equations without the body forces, free electric charges and magnetic charges and in terms of mechanical displacement components, electric potential and magnetic potential, carefully rearranging and considering the terms with the lowest order of r yields,

$$\begin{aligned}
 \frac{\partial^2 \hat{U}_0^{(m)}}{\partial \theta^2} + p_1 \frac{\partial \hat{U}_0^{(m)}}{\partial \theta} + p_2 \hat{U}_0^{(m)} + p_3 \frac{\partial^2 \hat{V}_0^{(m)}}{\partial \theta^2} + p_4 \frac{\partial \hat{V}_0^{(m)}}{\partial \theta} + p_5 \hat{V}_0^{(m)} + p_6 \frac{\partial^2 \hat{W}_0^{(m)}}{\partial \theta^2} + p_7 \frac{\partial \hat{W}_0^{(m)}}{\partial \theta} + p_8 \hat{W}_0^{(m)} \\
 + p_9 \frac{\partial^2 \hat{\Phi}_0^{(m)}}{\partial \theta^2} + p_{10} \frac{\partial \hat{\Phi}_0^{(m)}}{\partial \theta} + p_{11} \hat{\Phi}_0^{(m)} + p_{12} \frac{\partial^2 \hat{\Psi}_0^{(m)}}{\partial \theta^2} + p_{13} \frac{\partial \hat{\Psi}_0^{(m)}}{\partial \theta} + p_{14} \hat{\Psi}_0^{(m)} = 0, \quad (4a)
 \end{aligned}$$

$$\begin{aligned}
 \frac{\partial^2 \hat{V}_0^{(m)}}{\partial \theta^2} + q_1 \frac{\partial \hat{V}_0^{(m)}}{\partial \theta} + q_2 \hat{V}_0^{(m)} + q_3 \frac{\partial^2 \hat{U}_0^{(m)}}{\partial \theta^2} + q_4 \frac{\partial \hat{U}_0^{(m)}}{\partial \theta} + q_5 \hat{U}_0^{(m)} + q_6 \frac{\partial^2 \hat{W}_0^{(m)}}{\partial \theta^2} + q_7 \frac{\partial \hat{W}_0^{(m)}}{\partial \theta} + q_8 \hat{W}_0^{(m)} \\
 + q_9 \frac{\partial^2 \hat{\Phi}_0^{(m)}}{\partial \theta^2} + q_{10} \frac{\partial \hat{\Phi}_0^{(m)}}{\partial \theta} + q_{11} \hat{\Phi}_0^{(m)} + q_{12} \frac{\partial^2 \hat{\Psi}_0^{(m)}}{\partial \theta^2} + q_{13} \frac{\partial \hat{\Psi}_0^{(m)}}{\partial \theta} + q_{14} \hat{\Psi}_0^{(m)} = 0, \quad (4b)
 \end{aligned}$$

$$\begin{aligned} & \frac{\partial^2 \hat{W}_0^{(m)}}{\partial \theta^2} + r_1 \frac{\partial \hat{W}_0^{(m)}}{\partial \theta} + r_2 \hat{W}_0^{(m)} + r_3 \frac{\partial^2 \hat{U}_0^{(m)}}{\partial \theta^2} + r_4 \frac{\partial \hat{U}_0^{(m)}}{\partial \theta} + r_5 \hat{U}_0^{(m)} + r_6 \frac{\partial^2 \hat{V}_0^{(m)}}{\partial \theta^2} + r_7 \frac{\partial \hat{V}_0^{(m)}}{\partial \theta} + r_8 \hat{V}_0^{(m)} \\ & + r_9 \frac{\partial^2 \hat{\Phi}_0^{(m)}}{\partial \theta^2} + r_{10} \frac{\partial \hat{\Phi}_0^{(m)}}{\partial \theta} + r_{11} \hat{\Phi}_0^{(m)} + r_{12} \frac{\partial^2 \hat{\Psi}_0^{(m)}}{\partial \theta^2} + r_{13} \frac{\partial \hat{\Psi}_0^{(m)}}{\partial \theta} + r_{14} \hat{\Psi}_0^{(m)} = 0, \end{aligned} \quad (4c)$$

$$\begin{aligned} & \frac{\partial^2 \hat{\Phi}_0^{(m)}}{\partial \theta^2} + s_1 \frac{\partial \hat{\Phi}_0^{(m)}}{\partial \theta} + s_2 \hat{\Phi}_0^{(m)} + s_3 \frac{\partial^2 \hat{U}_0^{(m)}}{\partial \theta^2} + s_4 \frac{\partial \hat{U}_0^{(m)}}{\partial \theta} + s_5 \hat{U}_0^{(m)} + s_6 \frac{\partial^2 \hat{V}_0^{(m)}}{\partial \theta^2} + s_7 \frac{\partial \hat{V}_0^{(m)}}{\partial \theta} + s_8 \hat{V}_0^{(m)} \\ & + s_9 \frac{\partial^2 \hat{W}_0^{(m)}}{\partial \theta^2} + s_{10} \frac{\partial \hat{W}_0^{(m)}}{\partial \theta} + s_{11} \hat{W}_0^{(m)} + s_{12} \frac{\partial^2 \hat{\Psi}_0^{(m)}}{\partial \theta^2} + s_{13} \frac{\partial \hat{\Psi}_0^{(m)}}{\partial \theta} + s_{14} \hat{\Psi}_0^{(m)} = 0, \end{aligned} \quad (4d)$$

$$\begin{aligned} & \frac{\partial^2 \hat{\Psi}_0^{(m)}}{\partial \theta^2} + t_1 \frac{\partial \hat{\Psi}_0^{(m)}}{\partial \theta} + t_2 \hat{\Psi}_0^{(m)} + t_3 \frac{\partial^2 \hat{U}_0^{(m)}}{\partial \theta^2} + t_4 \frac{\partial \hat{U}_0^{(m)}}{\partial \theta} + t_5 \hat{U}_0^{(m)} + t_6 \frac{\partial^2 \hat{V}_0^{(m)}}{\partial \theta^2} + t_7 \frac{\partial \hat{V}_0^{(m)}}{\partial \theta} + t_8 \hat{V}_0^{(m)} \\ & + t_9 \frac{\partial^2 \hat{W}_0^{(m)}}{\partial \theta^2} + t_{10} \frac{\partial \hat{W}_0^{(m)}}{\partial \theta} + t_{11} \hat{W}_0^{(m)} + t_{12} \frac{\partial^2 \hat{\Phi}_0^{(m)}}{\partial \theta^2} + t_{13} \frac{\partial \hat{\Phi}_0^{(m)}}{\partial \theta} + t_{14} \hat{\Phi}_0^{(m)} = 0, \end{aligned} \quad (4e)$$

where p_i , q_i , r_i , s_i and t_i ($i=1\sim 14$) are known functions of θ .

Equations (4) are a set of ordinary differential equations with variable coefficients that depend only on θ , and the three displacement components, electric potential and magnetic potential are generally coupled. The exact closed-form solutions to Eqs. (4) are intractable, if they exist. The power series method can be directly adopted to develop a general solution for ordinary differential equations with variable coefficients. Very high-order terms must be considered to obtain an accurate solution and this requirement can cause numerical difficulties. To overcome these difficulties, a domain decomposition technique is used in conjunction with the power series method to establish a general solution of Eqs. (4).

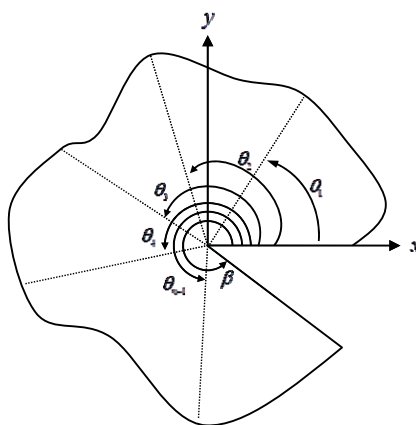


Fig. 2 Sub-domains for $\theta \in [0, \beta]$

The range of θ under consideration is first divided into a number of sub-domains (see Fig. 2). A series solution to Eqs. (4) is established in each sub-domain. Consequently, a general solution cover the whole θ domain is constructed from these series solutions in the sub-domains by imposing the continuity conditions between each pair of adjacent sub-domains. This process is a very convenient means of constructing solutions that can be used to analyze multi-material wedges, which are also considered in this work.

To establish the power series solution for sub-domain i where $\theta_{i-1} \leq \theta \leq \theta_i$, the variable coefficients in Eqs. (4) are expanded in terms of the power series of θ with respect to the middle point of the sub-domain, $\bar{\theta}_i$:

$$p_j(\theta) = \sum_{k=0}^K (\chi_j)_k^{(i)} (\theta - \bar{\theta}_i)^k, q_j(\theta) = \sum_{k=0}^K (\kappa_j)_k^{(i)} (\theta - \bar{\theta}_i)^k, r_j(\theta) = \sum_{k=0}^K (\varrho_j)_k^{(i)} (\theta - \bar{\theta}_i)^k,$$

$$s_j(\theta) = \sum_{k=0}^K (\xi_j)_k^{(i)} (\theta - \bar{\theta}_i)^k, t_j(\theta) = \sum_{k=0}^K (\zeta_j)_k^{(i)} (\theta - \bar{\theta}_i)^k. \quad (5)$$

Similarly, the solutions to Eqs. (4) in the sub-domain are expressed as

$$\hat{U}_{oi}^{(m)} = \sum_{j=0}^J \hat{A}_j^{(i)} (\theta - \bar{\theta}_i)^j, \hat{V}_{oi}^{(m)} = \sum_{j=0}^J \hat{B}_j^{(i)} (\theta - \bar{\theta}_i)^j, \hat{W}_{oi}^{(m)} = \sum_{j=0}^J \hat{C}_j^{(i)} (\theta - \bar{\theta}_i)^j,$$

$$\hat{\Phi}_{oi}^{(m)} = \sum_{j=0}^J \hat{D}_j^{(i)} (\theta - \bar{\theta}_i)^j, \hat{\Psi}_{oi}^{(m)} = \sum_{j=0}^J \hat{E}_j^{(i)} (\theta - \bar{\theta}_i)^j. \quad (6)$$

Substituting Eqs. (5) and (6) into Eqs. (4) yields the recurrence relations among the coefficients in Eqs. (6), and the coefficients $\hat{A}_j^{(i)}, \hat{B}_j^{(i)}, \hat{C}_j^{(i)}, \hat{D}_j^{(i)}$ and $\hat{E}_j^{(i)}$ with $j \geq 2$ are determined from the recurrence relations if $\hat{A}_0^{(i)}, \hat{A}_1^{(i)}, \hat{B}_0^{(i)}, \hat{B}_1^{(i)}, \hat{C}_0^{(i)}, \hat{C}_1^{(i)}, \hat{D}_0^{(i)}, \hat{D}_1^{(i)}, \hat{E}_0^{(i)}$ and $\hat{E}_1^{(i)}$ are known. Accordingly, the series solutions in sub-domain i are obtained with ten coefficients $\hat{A}_0^{(i)}, \hat{A}_1^{(i)}, \hat{B}_0^{(i)}, \hat{B}_1^{(i)}, \hat{C}_0^{(i)}, \hat{C}_1^{(i)}, \hat{D}_0^{(i)}, \hat{D}_1^{(i)}, \hat{E}_0^{(i)}$ and $\hat{E}_1^{(i)}$ to be determined.

When the range of θ is decomposed into n sub-domains, a total of $10n$ coefficients must be determined in all of the sub-domain solutions that are constructed using the above procedure. These solutions must satisfy the continuity conditions between pairs of adjacent sub-domains. These include continuities of tractions, mechanical displacements, electric displacements, electric potential and magnetic potential. These continuity conditions yield $10(n-1)$ algebraic equations. Homogenous boundary conditions at $\theta = 0$ and $\theta = \beta$ must be satisfied, yielding another ten equations. As a result, $10n$ coefficients are to be determined from $10n$ homogenous algebraic equations. A nontrivial solution for the coefficients yields a $10n \times 10n$ matrix with a determinant of zero. The roots of the zero determinant (λ_m), which can be complex

numbers, are obtained herein using the numerical approach of Müller (1956); they are ordered as $\text{Re}[\lambda_i] \leq \text{Re}[\lambda_{i+1}]$ ($i=1, 2, 3, \dots$).

3. VERIFICATION OF SOLUTION

To validate the proposed solution, convergence studies for $\text{Re}[\lambda_1]$ (real part of λ_1) are conducted by increasing the number of sub-domains or increasing the number of polynomial terms in each sub-domain, and the convergent solution is compared with the published result. The wedge under consideration is made of BaTiO₃-CoFe₂O₄ particulate composite, which is a typical MEE material. According to the macroscopic mixture rule, the composite material properties of this MEE material are related to the material properties of BaTiO₃ and CoFe₂O₄ by (Song and Sih 2003)

$$\bar{\kappa}_{ij} = \bar{\kappa}_{ij}^B V_l + \bar{\kappa}_{ij}^F (1 - V_l), \quad (7)$$

where $\bar{\kappa}_{ij}^B$ and $\bar{\kappa}_{ij}^F$ denote the material properties of BaTiO₃ and CoFe₂O₄ (Table 1), respectively, and V_l is the volume fraction of the inclusion BaTiO₃. The material properties in Table 1 were taken from Wang *et al.* (2011).

The homogeneous boundary conditions can be specified as follows: (1) mechanical boundary conditions, $\sigma_{r\theta} = \sigma_{\theta\theta} = \sigma_{z\theta} = 0$ (traction free) or $u_r = u_\theta = u_z = 0$ (clamped); (2) magneto-electrical boundary conditions, $D_\theta = B_\theta = 0$ (magneto-electrically open) or $\phi = \psi = 0$ (magneto-electrically closed). For simplicity, four letters are utilized to specify the boundary conditions along the two radial side faces of a wedge with vertex angle β . The first and third letters indicate mechanical boundary conditions at $\theta = 0$ and $\theta = \beta$, respectively; C and F specify clamped and traction-free, respectively. Similarly, the second and fourth letters represent the magneto-electric boundary conditions at $\theta = 0$ and $\theta = \beta$, respectively; C and O denote magneto-electrically closed and open boundary conditions, respectively.

To compare with the published result, the convergence study is conducted for an MEE wedge with $\beta = 360^\circ$ and having polarization direction along the z axis. For such a wedge, the out-of-plane deformation and in-plane electric and magnetic fields are independent of in-plane deformation and out-of-plane electric and magnetic fields. The wedge is made of BaTiO₃ and CoFe₂O₄ with $V_l = 50\%$ for $0^\circ \leq \theta < 180^\circ$ and with $V_l = 20\%$ for $180^\circ < \theta \leq 360^\circ$ and has FOFO boundary conditions. Notably, for comparison, $\bar{\mu}_{11} = 100 \times 10^{-6} \text{Ns}^2 / \text{C}^2$ for CoFe₂O₄, as in the work of Liu and Chue (2006), was used for the results in Table 2, which shows the results obtained using different numbers of sub-domains and polynomial terms for each sub-domain. Table 2 demonstrates that the convergent result, which is consistent with the result of Liu and Chue (2006), could be obtained by increasing the number of sub-domains or the number of polynomial terms for each sub-domain.

4. NUMERICAL RESULTS

This section presents numerical results of $\text{Re}[\lambda_1]$, taking into account the effects of material components, boundary conditions, polarization direction and geometry on the strength of the singularities of stress, electric displacement and magnetic flux. When λ_1 shown in a figure are all real, λ_1 , rather than $\text{Re}[\lambda_1]$, is used to label vertical axis of the

Table 1 Material properties

Parameters	BaTiO ₃ [#]	CoFe ₂ O ₄ [#]
\bar{c}_{11} (GPa)	166	286.0
\bar{c}_{12} (GPa)	77	173.0
\bar{c}_{13} (GPa)	78	170.5
\bar{c}_{33} (GPa)	162	269.5
\bar{c}_{44} (GPa)	43	45.3
\bar{e}_{15} (C/m ²)	11.6	0.
\bar{e}_{31} (C/m ²)	-4.4	0.
\bar{e}_{33} (C/m ²)	18.6	0.
\bar{d}_{15} (N/Am)	0.	550.0
\bar{d}_{31} (N/Am)	0.	580.3
\bar{d}_{33} (N/Am)	0.	699.7
$\bar{\eta}_{11}$ (C ² /Nm ²)	112.0×10 ⁻¹⁰	0.8×10 ⁻¹⁰
$\bar{\eta}_{33}$ (C ² /Nm ²)	126.0×10 ⁻¹⁰	0.93×10 ⁻¹⁰
$\bar{\mu}_{11}$ (Ns ² /C ²)	5.0×10 ⁻⁶	590.0×10 ⁻⁶
$\bar{\mu}_{33}$ (Ns ² /C ²)	10.0×10 ⁻⁶	157.0×10 ⁻⁶
\bar{g}_{11} (Ns/VC)	0.	0.
\bar{g}_{33} (Ns/VC)	0.	0.

Note: #: data from Wang *et al.* (2011).

figure. The numerical results herein were obtained by dividing the whole domain of θ into eight sub-domains and using series solutions that comprise ten terms for each sub-domain. The \bar{x} - \bar{y} - \bar{z} coordinate system is formed by rotating the x - y - z coordinate system counter-clockwise about the y -axis through an angle γ_y , so the angle between the polarization direction of an MEE wedge and its thickness direction is γ_y .

Table 2 Convergence of $\text{Re}[\lambda_1]$ for an MEE wedge

Number of Sub-domains	Terms					Liu and Chue (2006)
	6	8	10	12	15	
3	0.4978	0.4417	0.4998	0.4750	0.4999	
4	0.4963	0.4999	0.4984	0.4999	0.4999	
6	0.4993	0.4999	0.5000	0.4999	0.5000	0.5000
8	0.4999	0.4999	0.5000	0.5000	0.5000	

4.1 Wedges made of a single MEE material

Figure 3 shows $\text{Re}[\lambda_1]$ for $\text{BaTiO}_3\text{-CoFe}_2\text{O}_4$ wedges with $V_f = 20\%$, $\beta = 270^\circ$ and different boundary conditions varying with γ_y , while Fig. 4 displays the results for wedges with $\beta = 360^\circ$. As expected, the results are symmetric with respect to $\gamma_y = 90^\circ$. Changing the polarization direction may cause λ_1 changing from real numbers to complex numbers and vice versa. For example, λ_1 for FCFC wedges are complex for $44^\circ \leq \gamma_y \leq 136^\circ$. Gradually changing γ_y from 0° to 90° leads the increase or decrease of $\text{Re}[\lambda_1]$, depending on β and boundary conditions. Varying γ_y results in larger changes of $\text{Re}[\lambda_1]$ for FCFC and COCO wedges with $\beta = 270^\circ$ than those for wedges with $\beta = 360^\circ$, and the change can reach 9%.

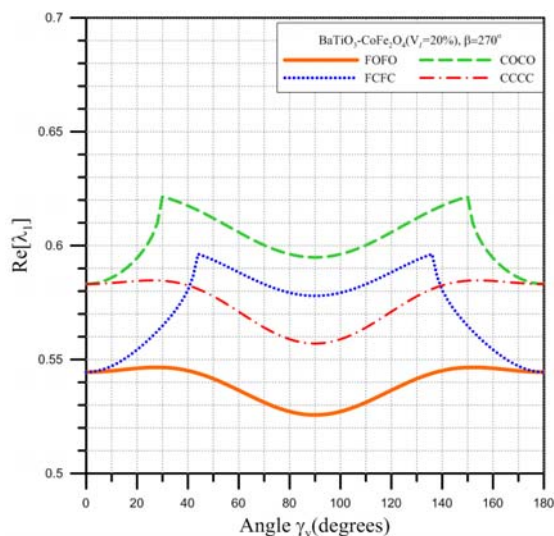


Fig. 3 Variation of $\text{Re}[\lambda_1]$ with polarization direction for MEE wedges with $\beta = 270^\circ$

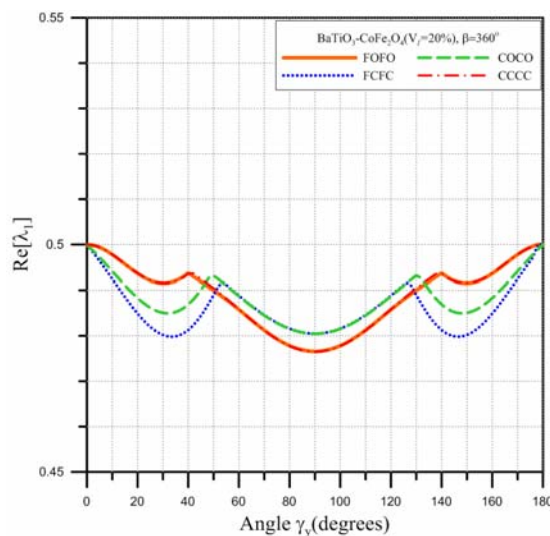


Fig. 4 Variation of $\text{Re}[\lambda_1]$ with polarization direction for MEE wedges with $\beta = 360^\circ$

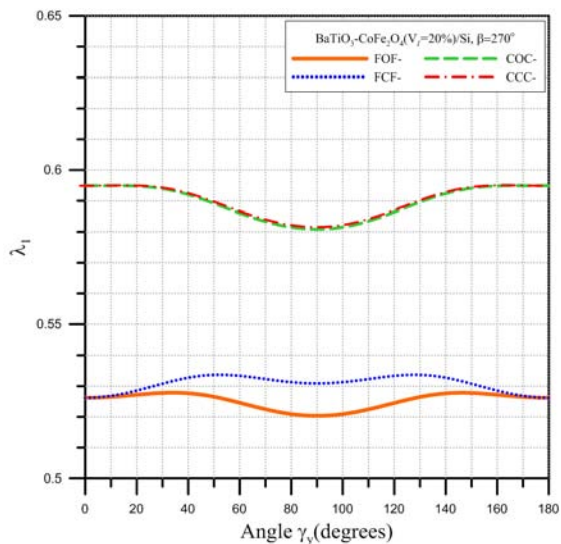


Fig. 5 Variation of $\text{Re}[\lambda_1]$ with polarization direction for MEE/Si wedges with $\beta = 270^\circ$

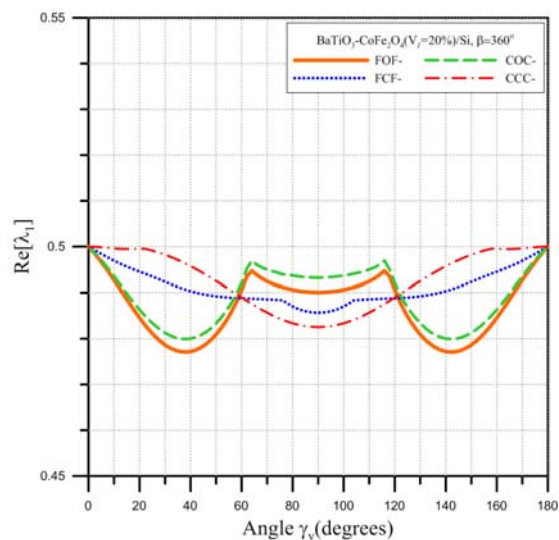


Fig. 6 Variation of $\text{Re}[\lambda_1]$ with polarization direction for MEE/Si wedges with $\beta = 360^\circ$

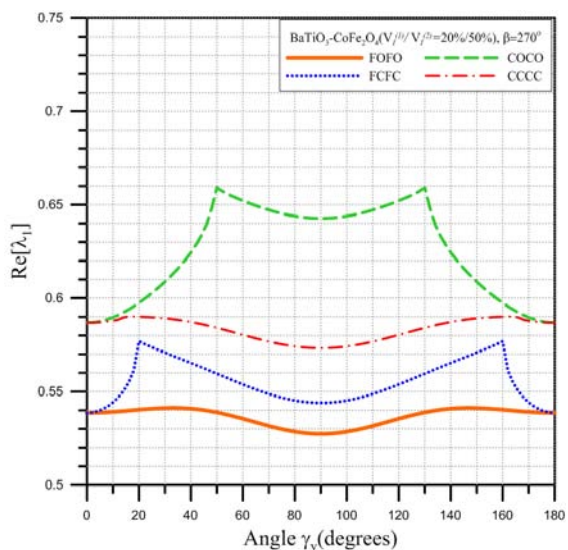


Fig. 7 Variation of $\text{Re}[\lambda_1]$ with polarization direction for MEE/MEE wedges with $\beta = 270^\circ$

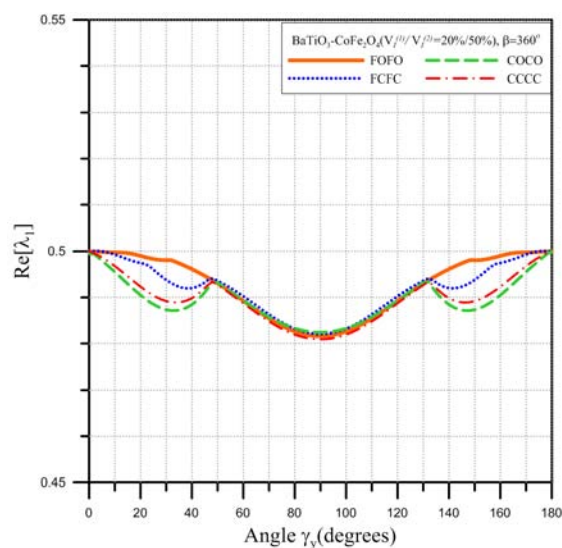


Fig. 8 Variation of $\text{Re}[\lambda_1]$ with polarization direction for MEE/MEE wedges with $\beta = 360^\circ$

4.2 Bi-material Wedges

This section concerns bi-material wedges with the same geometry as those considered in the preceding section. Figures 5 and 6 show $\text{Re}[\lambda_1]$ varying with γ_y for $\text{BaTiO}_3\text{-CoFe}_2\text{O}_4/\text{Si}$ wedges, in which Si is in the region of $\beta - 180^\circ < \theta \leq \beta$, while Figs. 7 and 8 illustrate the results for wedges made of $\text{BaTiO}_3\text{-CoFe}_2\text{O}_4$ with $V_f = 50\%$ in $0^\circ \leq \theta < 180^\circ$ and $\text{BaTiO}_3\text{-CoFe}_2\text{O}_4$ with $V_f = 20\%$ in $180^\circ < \theta \leq \beta$. Notably, when specifying the boundary conditions in Figs. 5 and 6, “-” denotes the absence of any magneto-electrical boundary conditions at $\theta = \beta$.

Figure 5 shows that λ_1 for wedges with $\beta = 270^\circ$ are all real, and different polarization directions cause small changes of λ_1 with less than 3%. It is interesting to observe that λ_1 for wedges with COC- boundary conditions are very close to those for wedges with CCC- boundary conditions. Free-free boundary conditions result in more severe singularities than clamped-clamped boundary conditions. However, these observations are not valid to the results for wedges with $\beta = 360^\circ$ in Fig. 6. The orientation of polarization may change the order of the singularity by approximately 5%. Comparing Figs. 5 and 6 with Figs. 3 and 4, respectively, discovers that bi-material wedges with $\beta = 270^\circ$ and free-free mechanical boundary conditions have stronger singularities than wedges made of a single MEE material, while wedges with CCC boundary conditions show an opposite trend, which is also observed for wedges with $\beta = 360^\circ$ and CCC boundary conditions.

Figure 7 demonstrates that changing the direction of polarization can change $\text{Re}[\lambda_1]$ by up to approximately 10% for wedges with $\beta = 270^\circ$ and COCO boundary conditions, while the changes of $\text{Re}[\lambda_1]$ are less than 3% for wedges with FOFO and CCC boundary conditions. Figure 8 discloses that varying the direction of polarization only change $\text{Re}[\lambda_1]$ of wedges with $\beta = 360^\circ$ and different boundary conditions by less than 4%. Comparing Fig. 8 with Fig. 4 finds that bi-material MEE wedges with $\beta = 360^\circ$ yield less severe singularities than do wedges made of a single MEE material.

5. CONCLUSIONS

This study found an asymptotic solution to an MEE wedge to investigate geometrically-induced magneto-electro-elastic singularities at the vertex of the wedge based on three-dimensional magneto-electro-elasticity theory in a cylindrical coordinate system. The piezoelectric material has an arbitrary direction of polarization. The solution was obtained using an eigenfunction expansion approach in conjunction with a power series technique to the three-dimensional equations of motion and Maxwell's equations, which are five coupled partial differential equations in terms of the displacement components and electric and magnetic potentials. The solutions were validated by performing convergence studies of $\text{Re}[\lambda_1]$ for a $\text{BaTiO}_3\text{-CoFe}_2\text{O}_4$ wedge with polarization in the thickness direction, and comparing the convergent $\text{Re}[\lambda_1]$ with the result published for a wedge under anti-plane deformation and in-plane electric and magnetic fields.

The proposed solution was employed to examine singularities in wedges that comprise a single magneto-electro-elastic material ($\text{BaTiO}_3\text{-CoFe}_2\text{O}_4$), bounded MEE/isotropic elastic materials ($\text{BaTiO}_3\text{-CoFe}_2\text{O}_4/\text{Si}$), or MEE/MEE materials ($\text{BaTiO}_3\text{-CoFe}_2\text{O}_4 (V_f = 50\%) / \text{BaTiO}_3\text{-CoFe}_2\text{O}_4 (V_f = 20\%)$). The value of $\text{Re}[\lambda_1]$, which is directly related to the order of the singularity, is displayed for different wedge angles, combinations of boundary conditions, and directions of polarization. As expected, the polarization direction may significantly affect $\text{Re}[\lambda_1]$.

ACKNOWLEDGEMENT

The authors would like to thank the National Science Council of the Republic of China, Taiwan, for financially supporting this research under Contract No. NSC 102-2221-E-009-071.

REFERENCES

- Bogy, D.B and Wang, K.C. (1971), "Stress singularities at interface corners in bonded dissimilar isotropic elastic materials," *Int. J. Solids Struct.*, Vol. 7, 993-1005.
- Burton, W.S. and Sinclair, G.B. (1986), "On the singularities in Reissner's theory for the bending of elastic plates," *J. Appl. Mech.*, Vol. 53(1), 220-222.
- Chen, M.C. and Ping, X.C. (2007), "Finite element analysis of piezoelectric corner configurations and cracks accounting for different electrical permeabilities," *Eng. Fracture Mech.*, Vol. 74(9), 1511-1524.
- Chen, M.C, Zhu, J.J. and Sze, K.Y. (2006), "Electroelastic singularities in piezoelectric-elastic wedges and junctions," *Eng. Fracture Mech.*, Vol. 73(7), 855-868.
- Chen, T.H., Chue, C.H. and Lee, H.T. (2004), "Stress singularities near the apex of a cylindrically polarized piezoelectric wedge," *Arch. Appl. Mech.*, Vol. 74 (3-4), 248-261.
- Chue, C.H. and Chen, C.D. (2002), "Decoupled formulation of piezoelectric elasticity under generalized plane deformation and its application to wedge problems," *Int. J. Solids Struct.*, Vol. 39(12), 3131-3158.
- Chue, C.H. and Chen, C.D. (2003), "Antiplane stress singularities in a bonded bimaterial piezoelectric wedge," *Arch. Appl. Mech.*, Vol. 72(9), 673-685.
- Dempsey, J.P. and Sinclair, G.B. (1979), "On the stress singularities in the plate elasticity of the composite wedge," *J. Elast.*, Vol. 9(4), 373-391.
- Hartranft, R.J. and Sih, G.C. (1969), "The use of eigenfunction expansions in the general solution of three-dimensional crack problems," *J. Math. Mech.*, Vol. 19, 123-138.

- Huang, C.S. (2002), "On the singularity induced by boundary conditions in a third-order thick plate theory," *J. Appl. Mech., ASME*, Vol. 69(6), 800-810.
- Huang, C.S. (2003), "Stress singularities at angular corners in first-order shear deformation plate theory," *Int. J. Mech. Sci.*, Vol. 45(1), 1-20.
- Huang, C.S. (2004), "Corner stress singularities in a high-order plate theory," *Comput. Struct.*, Vol. 82, 1657-1669.
- Huang, C.S. and Chang, M.J. (2007), "Corner stress singularities in a FGM thin plate," *Int. J. Solids Struct.*, Vol.44(9), 2802-2819.
- Huang, C.S. and Hu, C.N. (2013), "Three-dimensional analyses of stress singularities at the vertex of a piezoelectric wedge," *Appl. Math. Model.*, Vol.37(6), 4517-4537
- Hwu, C. and Ikeda, T. (2008), "Electromechanical fracture analysis for corners and cracks in piezoelectric materials," *Int. J. Solids Struct.*, Vol. 45(22-23), 5744-5764
- Lin, Y.Y. and Sung, J.C. (1998), "Stress singularities at the apex of a dissimilar anisotropic wedge," *J. Appl. Mech., ASME*, Vol.65(2), 454-463.
- Liu, T.J.C. (2009), "The singularity problem of the magneto-electro-elastic wedge-junction structure with consideration of the air effect," *Arch. Appl. Mech.*, Vol.79(5), 377-393.
- Liu, T.J.C. and Chue, C.H. (2006), "On the singularities in a bimaterial magneto-electro-elastic composite wedge under antiplane deformation," *Composite Struct.*, Vol.72(2), 254-265.
- McGee, O.G. and Kim, J.W. (2005), "Sharp corners functions for Mindlin plates," *J. Appl. Mech., ASME*, Vol.72(1), 1-9.
- Müller, D.E. (1956), "A method for solving algebraic equations using an automatic computer," *Mathematical Tables and Aids to Computation*, Vol. 10, 208-215.
- Ojikutu, I.O., Low, R.O. and Scott, R.A. (1984), "Stress singularities in laminated composite wedge," *Int. J. Solids Struct.*, Vol. 20, 777-790.
- Rao, A.K. (1971), "Stress concentrations and singularities at interfaces corners," *Z. Angew. Math. Mech.*, Vol. 51, 395-406.
- Scherzer, M. and Kuna, M. (2004), "Combined analytical and numerical solution of 2D interface corner configurations between dissimilar piezoelectric materials," *Int. J. Fracture*, Vol.127(1), 61-99.
- Shang, F. and Kitamura, T. (2005), "On stress singularity at the interface edge between piezoelectric thin film and elastic substrate," *Microsys. Technol.*, Vol. 11(8-10), 1115-1120.
- Sinclair, G.B. (2004), "Stress singularities in classical elasticity—I: removal, interpretation, and analysis," *Appl. Mech. Rev.*, 57(4), 251-297.

- Song, Z.F. and Sih, G.C. (2003), "Crack initiation behavior in magnetoelastic composite under in-plane deformation," *Theor. Appl. Fracture Mech.*, 39(3), 189-207
- Sue, W.C., Liou, J.Y. and Sung, J.C. (2007), "Investigation of the stress singularity of a magnetoelastic bonded antiplane wedge," *Appl. Math. Model.*, Vol. 31(10), 2313-2331.
- Ting, T.C.T. and Chou, S.C. (1981), "Edge singularities in anisotropic composites," *Int. J. Solids Struct.*, Vol.17(11):, 1057-1068.
- Wang, Y., Xu, R. and Ding, H. (2011), "Axisymmetric bending of functionally graded circular magneto-electro-elastic plates," *Eur. J. Mech. A*, Vol. 30(6), 999-1011.
- Wang, Z. and Zheng, B. (1995), "The general solution of three dimensional problems in piezoelectric media," *Int. J. Solids Struct.*, Vol.32(1), 105-115.
- Williams, M.L. (1952a), "Stress singularities resulting from various boundary conditions in angular corners of plates under bending," *Proceeding of 1st U.S. National Congress of Applied Mechanics*.
- Williams, M.L. (1952b), "Stress singularities resulting from various boundary conditions in angular corners of plates in extension," *J. Appl. Mech.*, 19, 526-528.
- Xie, M. and Chaudhuri, R.A. (1997), "Three-dimensional stress singularity at a bimaterial interface crack front," *Composite Struct.*, Vol.40(2), 137-147.
- Xu, X.L. and Rajapakse, R.K.N.D. (2000), "On singularities in composite piezoelectric wedges and junctions," *Int. J. Solids Struct.*, Vol.37(23), 3235-3275.